Interlayer phonons and *c*-axis charge response in the high-temperature superconductors

2002 J. Phys.: Condens. Matter 14 3239

(http://iopscience.iop.org/0953-8984/14/12/312)

INSTITUTE OF PHYSICS PUBLISHING JOURNAL OF PHYSICS: CONDENSED MATTER

J. Phys.: Condens. Matter **14** (2002) 3239–3257 PII: S0953-8984(02)32342-7

Interlayer phonons and *c*-axis charge response in the high-temperature superconductors

Claus Falter, Georg A Hoffmann and Frank Schnetgöke

Institut für Festkörpertheorie, Universität Münster, Wilhelm-Klemm-Straße 10, 48149 Münster, Germany

E-mail: Falter@nwz.uni-muenster.de

Received 4 January 2002
Published 15 March 2002
Online at stacks.iop.org/JPhysCM/14/3239

Abstract

Interlayer phonons are useful probes for getting more insight into the charge response across the CuO_2 planes of the high-temperature superconductors (HTSC), which is a matter of controversial in the literature, because the type of charge response is reflected by characteristic signatures of the phonons. In this context we investigate the question of whether *c*-axis phonons are expected to show metallic or insulating response behaviour. Formerly obtained qualitative results for La_2CuO_4 are made quantitative by generalizing our previously developed description of the charge response and screening in the HTSC in terms of charge fluctuations (CF) taking additionally dipole fluctuations (DF) into account. Calculations are performed of the *c*-axis phonon dispersion for different values of the *c*-axis plasmon frequency in order to model different anisotropies of the material. In this way the effect of the charge response caused by both CF and DF is investigated from the static, adiabatic case to the dynamic, nonadiabatic regime and compared with experimental results from neutron scattering and infrared spectroscopy. From the interpretation of the data, phonon–plasmon mixing becomes very likely. The three dimensionality due to direct Coulomb interaction and dielectric coupling by DF between the layers is shown to be important. Moreover, we calculate for characteristic *c*-axis modes in the extended model including both CF and DF the displacement-induced self-consistent changes of the crystal potential that is a suitable measure for the strength of electron–phonon coupling.

1. Introduction

The nature of the *c*-axis charge response of the layered high-temperature superconductors (HTSC) is still not well understood. Band-structure calculations for the cuprates always predict an appreciable *c*-axis dispersion and thus an anisotropic three-dimensional metallic state [1]. In contrast to this Fermi-liquid-based approach, the Luttinger-liquid model proposes that the

charge carriers are confined to the CuO_2 planes [2]. However, a strictly two-dimensional model *a priori* neglects the three dimensionality of the real materials resulting from direct Coulomb interaction and dielectric coupling between the layers. These interactions prove to be important for a quantitative description of the lattice dynamics and the electronic density response, as is demonstrated by our calculations.

A model, resting on the Fermi-liquid picture, recently proposed in an effort to classify the HTSC as regards their *c*-axis transport explains the experimental situation quite well [3]. Here the out-of-plane charge transport comes from an interplay of the coherent component due to wavefunction overlap (direct interlayer coupling), impurity-assisted hopping and phonon-(boson-) assisted interlayer hopping. The relative strength of the coherent and incoherent contributions varies for the HTSC depending on the degree of anisotropy, from fully oxygenated Y–Ba–Cu–O, which is one of the least anisotropic cuprates and nearly coherent, to the very anisotropic Bi-based cuprates, with a very weak direct interlayer coupling and which are nearly incoherent.

In this paper we study the effect of the anisotropy on the phonon dispersion along the *c*-axis (the Λ direction in the Brillouin zone) for La_2CuO_4 in terms of the coherent component of the *c*-axis charge response. We investigate phonon–plasmon mixing along the Λ direction for the relevant modes starting from the nonadiabatic soft-plasmon case of a nearly two-dimensional quasiparticle band structure and going up to the adiabatic limit of a less anisotropic metal as predicted typically by band-structure calculations within the local density approximation (LDA). Qualitatively, such coupling effects between a low-lying *c*-axis plasmon and the phonons have been analysed in our earlier work for La_2CuO_4; see [4]. In these calculations only ionic charge fluctuations (CF) have been considered as possible screening processes in the metallic phase, and the insulating phase of La_2CuO_4 was approximated by an *ab initio* rigid-ion model (RIM) without any further polarization degrees of freedom. So, only a restricted comparison of the theoretical results with the experimental neutron scattering data [5] was possible. For a discussion of phonon–plasmon mixing in the cuprates in the context of many-body polaronic effects in the phonon spectrum, we refer the reader to [6].

Quite recently, we have shown that screening in La_2CuO_4 and very likely in all HTSC is best described by a two-dimensional electronic structure in the CuO_2 plane with CF in that layer as the most important polarization process [7]. We find in these investigations an important contribution of anisotropic screening by dipole fluctuations (DF) between the layers moreover; the dipole polarizability dominates in the (ionic) *c*-direction. In particular, screening processes of this type prove to be very effective for the infrared-active A_{2u} modes polarized along the *c*-axis. The calculations performed in section 3 besides CF also take DF into account and allow for these polarization processes for the first time also in the nonadiabatic regime (dynamical screening). In this way a quantitative comparison with the current interpretation of the neutron data becomes possible and the apparent inconsistency between the optical experiments [8–10] and the neutron data [5] concerning the *c*-axis response already addressed qualitatively in [4] is reconciled.

As far as optimally doped and underdoped La–Cu–O is concerned, the optical *c*-axis spectra display features typical of an ionic insulator [8–10] and not of a metal. They are dominated by optical phonons and are almost unchanged from those of the insulator upon doping. The *c*-axis neutron data seem to contradict the optical *c*-axis results. While the phonon dispersion of undoped La_2CuO_4 also shows characteristic A_{2u} discontinuities typical of ionic insulators, in the doped metallic samples these splittings disappear and a phonon dispersion results along the Λ direction, which is typical for a three-dimensional anisotropic metal as calculated in the adiabatic approximation. Connected with the disappearance of the A_{2u} discontinuities in the metallic phase is the appearance of a characteristic phonon branch

of Λ_1 symmetry with a steep dispersion. This signature is predicted also by our calculations in the adiabatic approximation for the metallic phase.

In section 2 the necessary elements of the theory and modelling are sketched to improve the readability of the paper. In section 3 model calculations are performed for the c-axis phonon dispersion for different c-axis plasma frequencies, allowing for CF and DF as screening processes. These investigations clarify the type of charge response strictly along the c-axis and in its immediate vicinity and answer the question of whether c-axis-polarized phonons are expected to show metallic or insulating behaviour. Finally, our earlier calculations based on CF only [4] of the displacement-induced self-consistent changes of the electron–ion potential for the axial oxygen and the axial lanthanum breathing mode at the Z point, O_z^Z and La_z^Z, are extended, including additionally DF. Section 4 summarizes our results.

2. Review of the theory and modelling

HTSC are materials displaying an anisotropic mixed ionic–covalent (metallic) bonding. While the ionic nature of bonding predominates along the c-axis, covalent (metallic) bonding contributions become important in the CuO_2 plane.

A detailed description of our microscopic approach to the electronic density response, the lattice dynamics and the electron–phonon interaction (EPI) in the HTSC can be found for example in [11] and [12]. In this theory the ionic local part of the electronic charge response is approximated by an *ab initio* RIM, while the nonlocal, nonrigid part of the density response is modelled in a parameter-free fashion by electronic CF and DF of the ions. The covalent (metallic) features of bonding and screening in the HTSC are taken approximatively into account in terms of ion softening and CF via the electronic band structure—first, in a global way by using effective ionic charges in the RIM, as calculated from a tight-binding analysis of the (first-principles) electronic band structure and, secondly, through the electronic polarizability, which contains the kinetic one-particle contribution of the charge response. The latter is also calculated from the electronic band structure. In addition, scaling of the short-range part of the pair potentials between the ions is considered to simulate further covalence effects in the calculations [13]. Scaling is performed in such a way that the energy-minimized structure is as close as possible to the experimental one.

The tight-binding analysis supplies the effective ionic charges as extracted from the orbital occupation numbers Q_μ of the μ (tight-binding) orbital in question:

$$Q_\mu = \frac{2}{N} \sum_{n\vec{k}} |C_{\mu n}(\vec{k})|^2. \tag{1}$$

$C_{\mu n}(\vec{k})$ stands for the μ-component of the eigenvector of band n at the wavevector $\vec{k}$ in the first Brillouin zone; the summation in equation (1) runs over all occupied states and N gives the number of elementary cells in the (periodic) crystal. The RIM with the corrections just mentioned then serves as a reference system for the description of the HTSC. For a representation of the nonlocal (nonrigid) electronic density response and screening in the HTSC, particularly in the metallic phase, more or less localized electronic CF in the outer shells of the ions are considered. The latter dominate the long-range, nonlocal contribution of the electronic density response and the EPI in the HTSC. In addition, DF can be treated within our approach [12] and prove to be important in particular for the ions in the ionic layers. Thus, the starting point of our model is the ionic densities in the perturbed state which are given by

$$\rho_\alpha(\vec{r}) = \rho_\alpha^0(r) + \sum_\lambda Q_\lambda \rho_\lambda^{CF}(r) + \vec{p}_\alpha \cdot \hat{r}\, \rho_\alpha^D(r). \tag{2}$$

ρ_α^0 is the density of the unperturbed ion localized at the sublattice α of the crystal. The Q_λ and ρ_λ^{CF} describe the amplitudes and the form factors of the CF and the last term in equation (2) gives the dipolar deformation of an ion α with amplitude (dipole moment) $\vec{p}_\alpha$ and a radial density distribution ρ_α^D. $\hat{r}$ is the unit vector in the direction of $\vec{r}$. The ρ_λ^{CF} are approximated by a spherical average of the orbital densities of the outer ionic shells calculated in the LDA taking self-interaction effects into account. The dipole density ρ_α^D is obtained from a modified Sternheimer method in the framework of LDA-SIC (SIC standing for self-interaction corrections); see [12, 14, 15].

The total energy of the crystal is investigated by assuming that the density of the crystal can be approximated by a superposition of overlapping densities of the individual ions ρ_α. The ρ_α^0 are calculated within the LDA-SIC framework taking environment effects into account via a Watson sphere potential and also taking the calculated effective charges of the ions into account. Such an approximation holds well in the HTSC [13, 16]. Moreover, applying the pair-potential approximation we get for the total energy

$$E(R,\zeta) = \sum_{\vec{a}\alpha} E_\alpha^{\vec{a}}(\zeta) + \tfrac{1}{2}{\sum_{\substack{\vec{a}\alpha \\ \vec{b}\beta}}}' \phi_{\alpha\beta}(\vec{R}_\beta^{\vec{b}} - \vec{R}_\alpha^{\vec{a}}, \zeta). \tag{3}$$

The energy E depends on the configuration of the ions $\{R\}$ and the electronic degrees of freedom (EDF) $\{\zeta\}$ of the charge density, i.e. $\{Q_\lambda\}$ and $\{\vec{p}_\alpha\}$ in equation (2). $E_\alpha^{\vec{a}}$ are the energies of the single ions. $\vec{a}, \vec{b}$ denote the elementary cells in the crystal and α, β the sublattices. The second term in equation (3) is the interaction energy of the system, expressed as the pair interactions $\phi_{\alpha\beta}$. The prime in equation (3) means that the self-term has to be omitted. Both, $E_\alpha^{\vec{a}}$ and $\phi_{\alpha\beta}$ in general depend upon ζ via ρ_α.

From the adiabatic condition

$$\frac{\partial E(R,\zeta)}{\partial \zeta} = 0, \tag{4}$$

an expression for the force constants and, accordingly, the dynamical matrix in the harmonic approximation can be derived:

$$t_{ij}^{\alpha\beta}(\vec{q}) = [t_{ij}^{\alpha\beta}(\vec{q})]_{RIM} - \frac{1}{\sqrt{M_\alpha M_\beta}} \sum_{\kappa,\kappa'} [B_i^{\kappa\alpha}(\vec{q})]^* [C^{-1}(\vec{q})]_{\kappa\kappa'} B_j^{\kappa'\beta}(\vec{q}). \tag{5}$$

$[t_{ij}^{\alpha\beta}(\vec{q})]_{RIM}$ denotes the contribution of the RIM to the dynamical matrix. M_α, M_β are the masses of the ions and $\vec{q}$ is a wavevector from the first Brillouin zone. The quantities $\vec{B}(\vec{q})$ and $C(\vec{q})$ represent the Fourier transforms of the coupling coefficients as calculated from the energy:

$$\vec{B}_{\kappa\beta}^{\vec{a}\vec{b}} = \frac{\partial^2 E(R,\zeta)}{\partial \zeta_\kappa^{\vec{a}}\, \partial \vec{R}_\beta^{\vec{b}}}, \tag{6}$$

and

$$C_{\kappa\kappa'}^{\vec{a}\vec{b}} = \frac{\partial^2 E(R,\zeta)}{\partial \zeta_\kappa^{\vec{a}}\, \partial \zeta_{\kappa'}^{\vec{b}}}. \tag{7}$$

The derivatives in equations (6) and (7) have to be taken at the equilibrium positions. κ denotes the EDF (CF and DF in the present model) in an elementary cell of the crystal. The $\vec{B}$-coefficients describe the coupling between the EDF and the ions and the C-coefficients the interaction between the EDF. Equations (5)–(7) are generally valid and, in particular, are independent of our specific model for the decomposition of the perturbed density in equation (2) and of the pair approximation (3) for the energy.

The pair interactions $\phi_{\alpha\beta}$ can be decomposed into long-range Coulomb contributions and short-range terms. The latter are separated into: the interaction between the ion cores and the charge density from equation (2); the interaction between the density ρ_α and the density ρ_β (Hartree contribution); and a term representing the sum of the kinetic one-particle and the exchange–correlation contribution of the interaction between the two ions. A detailed description of the $\phi_{\alpha\beta}$ and the calculation of the coupling coefficients $\vec{B}$ and C for the EDF is given in [12]. In this context it should be mentioned that the matrix $C_{\kappa\kappa'}(\vec{q})$ of the EDF–EDF interaction whose inverse appears in equation (5) for the dynamical matrix can also be written as

$$C = \Pi^{-1} + \tilde{V}. \tag{8}$$

Π^{-1} contains the kinetic one-particle part of the interaction and $\tilde{V}$ the Hartree and exchange–correlation contribution. The quantity C^{-1} needed for the calculation of the dynamical matrix is closely related to the density response function (matrix) and to the inverse dielectric function (matrix) ε^{-1}. Writing this in matrix notation, we have the relation

$$C^{-1} = \Pi(1 + \tilde{V}\Pi)^{-1} \equiv \Pi\varepsilon^{-1}, \qquad \varepsilon = 1 + \tilde{V}\Pi. \tag{9}$$

The CF–CF submatrix of the matrix Π can be calculated approximatively from a tight-binding analysis of the (first-principles) electronic band structure. In this case the (static) electronic polarizability $\Pi(\vec{q}, \omega = 0)$, relevant for the adiabatic approximation of the phonons in the density response approach, is given by

$$\Pi_{\kappa\kappa'}(\vec{q}, \omega = 0) = -\frac{2}{N}\sum_{\substack{n,n' \\ \vec{k}}} \frac{f_{n'}(\vec{k}+\vec{q}) - f_n(\vec{k})}{E_{n'}(\vec{k}+\vec{q}) - E_n(\vec{k})}[C^*_{\kappa n}(\vec{k})C_{\kappa n'}(\vec{k}+\vec{q})][C^*_{\kappa' n}(\vec{k})C_{\kappa' n'}(\vec{k}+\vec{q})]^*. \tag{10}$$

f, E and C are the occupation numbers, the electronic quasiparticle band structure and the expansion coefficients of the Bloch functions in terms of the tight-binding functions.

The generalization for $\Pi = \Pi(\vec{q}, \omega \neq 0)$ needed in the nonadiabatic regime, where dynamical screening effects must be considered, can be achieved by adding $\hbar\omega + \mathrm{i}\eta$ to the differences of the 'single-particle energies' in the denominator of the expression for Π in equation (10). Using equation (9) for the dielectric function and the frequency-dependent version of the polarizability Π according to equation (10), the free-plasmon dispersion is obtained from the condition

$$\det[\varepsilon_{\kappa\kappa'}(\vec{q}, \omega)] = 0. \tag{11}$$

The coupled-mode frequencies of the phonons and the plasmon along the c-axis must be determined self-consistently from the secular equation for the dynamical matrix in equation (5), which now contains the frequency ω implicitly via Π in the quantity C^{-1} from equation (9).

The self-consistent change of the EDF $\zeta^{\vec{a}}_\kappa$, i.e. the CF and DF in our model, in a phonon mode $(\vec{q}\sigma)$ characterized by the displacements

$$\vec{u}^{\vec{a}}_\alpha(\vec{q}\sigma) = \left(\frac{\hbar}{2M_\alpha\omega_\sigma(\vec{q})}\right)^{1/2} \vec{e}^{\alpha}(\vec{q}\sigma)\mathrm{e}^{\mathrm{i}\vec{q}\cdot\vec{R}^{\vec{a}}} \equiv \vec{u}_\alpha(\vec{q}\sigma)\mathrm{e}^{\mathrm{i}\vec{q}\cdot\vec{R}^{\vec{a}}} \tag{12}$$

can be expressed in the form

$$\delta\zeta^{\vec{a}}_\kappa(\vec{q}\sigma) = \left[-\sum_\alpha \vec{X}^{\kappa\alpha}(\vec{q})\vec{u}_\alpha(\vec{q}\sigma)\right]\mathrm{e}^{\mathrm{i}\vec{q}\cdot\vec{R}^{\vec{a}}_\kappa} \equiv \delta\zeta_\kappa(\vec{q}\sigma)\mathrm{e}^{\mathrm{i}\vec{q}\cdot\vec{R}^{\vec{a}}}. \tag{13}$$

$\omega_\sigma(\vec{q})$ and $\vec{e}^{\alpha}(\vec{q}\sigma)$ are the phonon frequency and the polarization vector for the mode $(\vec{q}\sigma)$, and $\vec{X}^{\kappa\alpha}(\vec{q})$ describes the self-consistent reaction of the EDF in the phonon mode. It can be shown to be given by

$$\vec{X}(\vec{q}) = \Pi(\vec{q})\varepsilon^{-1}(\vec{q})\vec{B}(\vec{q}) = C^{-1}(\vec{q})\vec{B}(\vec{q}). \tag{14}$$

Finally, we introduce as a quantity that gives the strength of the EPI in a certain phonon mode—namely the change of the total self-consistent crystal potential felt by an electron—$\delta V_{eff}(\vec{r}, \vec{q}\sigma)$. Weighting this quantity with the corresponding density form factor $\rho_\kappa(\vec{r} - \vec{R}_\kappa^{\vec{a}})$ of the EDF located at $\vec{R}_\kappa^{\vec{a}}$ in the crystal, we get

$$\delta V_\kappa^{\vec{a}}(\vec{q}\sigma) = \int \mathrm{d}V \rho_\kappa\,(\vec{r} - \vec{R}_\kappa^{\vec{a}})\,\delta V_{eff}(\vec{r}, \vec{q}\sigma) \tag{15}$$

as a direct measure for the strength of electron–phonon coupling in the mode $(\vec{q}\sigma)$.

$\delta V_\kappa^{\vec{a}}(\vec{q}\sigma)$ can be expressed in terms of the coupling coefficients from equations (6), (7) in the following way:

$$\delta V_\kappa^{\vec{a}}(\vec{q}\sigma) = \left[\sum_\alpha \vec{W}_{\kappa\alpha}(\vec{q})\vec{u}_\alpha(\vec{q}\sigma)\right] \mathrm{e}^{\mathrm{i}\vec{q}\cdot\vec{R}_\kappa^{\vec{a}}} \equiv \delta V_\kappa(\vec{q}\sigma)\,\mathrm{e}^{\mathrm{i}\vec{q}\cdot\vec{R}^{\vec{a}}}, \tag{16}$$

where $\vec{W}(\vec{q})$ is the Fourier transform of

$$\vec{W}_{\kappa\beta}^{\vec{a}\vec{b}} = \vec{B}_{\kappa\beta}^{\vec{a}\vec{b}} - {}^{kin}\vec{B}_{\kappa\beta}^{\vec{a}\vec{b}} - \sum_{\vec{b}'\kappa'} \tilde{V}_{\kappa\kappa'}^{\vec{a}\vec{b}'} \vec{X}_{\kappa'\beta}^{\vec{b}'\vec{b}}. \tag{17}$$

${}^{kin}\vec{B}$ in equation (17) denotes the contribution of the kinetic energy to the coupling parameter $\vec{B}$ in equation (6).

3. Numerical results and discussion

3.1. Significance of dipole fluctuations for the c-axis response

The phonon dispersion along the $\Lambda \sim (0, 0, 1)$ direction of undoped La_2CuO_4 displays the typical LO–TO splittings of the A_{2u} modes (A_{2u} discontinuities) of an ionic insulator that have been observed by means of inelastic neutron scattering [5] as well as by infrared spectroscopy [8–10]. In doped metallic samples these splittings disappear in the current interpretation of the neutron experiments [5], so one should conclude that a conventional metallic charge response, well described by the static screening in the adiabatic approximation, arises during the insulator–metal transition. Moreover, in the metallic probes a characteristic branch of Λ_1 symmetry with a very steep dispersion is observed as a consequence of the closing of the A_{2u} splittings. In complete contrast to these observations are the results from infrared spectroscopy for during the insulator–metal transition [8–10]. The optical *c*-axis spectra display the typical features of an ionic insulator. They are dominated by optical A_{2u} phonons and are almost unchanged from the those of insulator upon doping. The most prominent feature of these spectra is the very large oscillator strength of one of the three A_{2u} modes with the intermediate frequency. We call this mode the 'ferroelectric mode' for reasons that will become clear below. The closing of the A_{2u} splitting of this mode would lead to the characteristic Λ_1 branch with the steep dispersion. For the consideration of the insulator–metal transition only the six z-polarized Λ_1 branches are of interest, because they are the only phonons that couple strongly with the CF [17]. At the Γ point of the Brillouin zone the Λ_1 modes yield one acoustic mode, three infrared-active optic A_{2u}^{Γ} modes and two Raman-active A_g^{Γ} modes (La^{Γ} and O_z^{Γ}), where the La or the O_z sublattice is displaced symmetrically with respect to the CuO_2 plane.

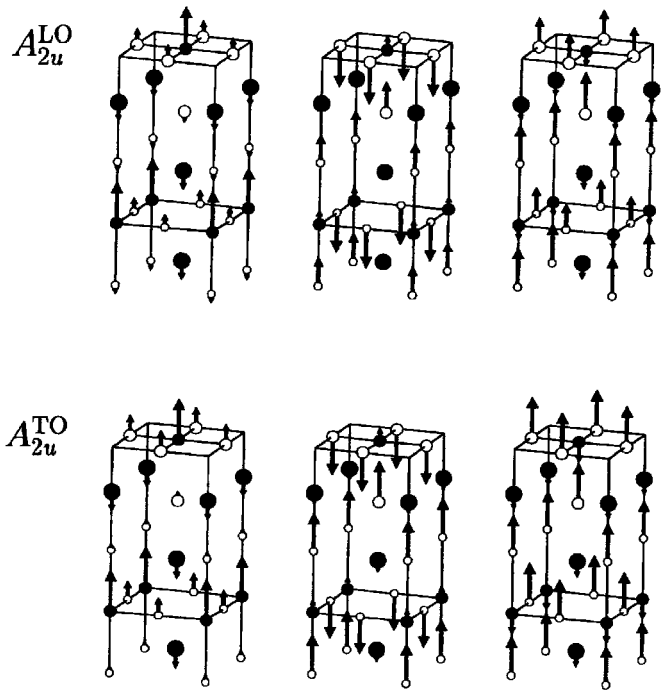

Figure 1. Displacement patterns of the three longitudinal and transverse optical A_{2u}^{Γ} modes of La_2CuO_4 at the Γ point as calculated with the RIM.

Table 1. Calculated frequencies in THz of the longitudinal and transverse A_{2u}^{Γ} modes in La_2CuO_4 as calculated with the rigid-ion model (RIM) and a model including additionally dipole fluctuations (AI) explained in the text. The sequence of the three TO–LO pairs corresponds to the sequence of the displacement patterns in figure 1.

	TO	LO	TO	LO	TO	LO
RIM	5.63	5.74	18.36	18.29	10.09	19.83
AI	4.52	5.25	14.14	12.62	6.61	17.18

In figure 1 we show the displacement patterns of the longitudinal and transverse optical A_{2u} modes for La_2CuO_4 at the Γ point as calculated with the RIM taking scaling of the short-range part of the Cu–O_{xy}, O_{xy}–La and O_z–La pair potentials and ion softening, as calculated from a tight-binding analysis of the electronic band structure, into account. This procedure leads to an excellent agreement with the experimental crystal structure [7]. Moreover, in table 1 we have listed the corresponding calculated phonon frequencies for the RIM and a model which contains additionally DF on the ions along the z-direction. The dipole polarizability of the ions has been calculated by the Sternheimer method in the framework of the DFT within the LDA including SIC effects. This model (adiabatic insulator: AI) is taken as a representative model of the insulating phase of La_2CuO_4. Note that in the Λ_1 branches, only DF along the z-direction are active; ones polarized in the x- or y-direction are forbidden by symmetry.

From the data calculated using the RIM as well as those from the AI model, we find a very large LO–TO splitting for the ferroelectric mode that is consistent with the gigantic

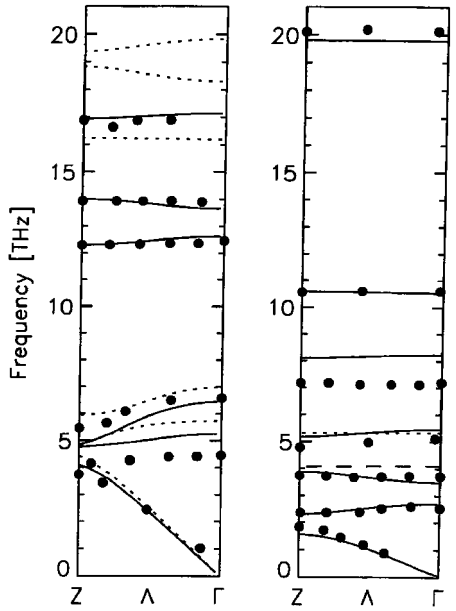

Figure 2. Calculated phonon dispersion for insulating La_2CuO_4 along the $\Lambda \sim (0, 0, 1)$ direction from Γ to $Z = (0, 0, 2\pi/c)$ as obtained with the AI model explained in the text with DF included. In the left-hand part the Λ_1 branches (——) together with the results from the RIM (– – –) are shown. The right-hand part displays the results for the remaining branches in the Λ direction Λ_2 (— — —) and Λ_3 (——). The dots represent the experimental results [5, 17].

oscillator strength for this mode seen in the infrared spectra. The 'ferroelectricity' is obvious from the displacement pattern given in figure 1. We see that in this strong mode the Cu and La cations vibrate against the O_{xy} and O_z anions and as a consequence the dipole moments generated by the motion of the ions add constructively to a large value. This mode will carry nearly all contributions to the static dielectric constant along the c-direction. For more details concerning the infrared response in La_2CuO_4, we refer the reader to [7], where, in addition to the macroscopic high-frequency dielectric tensor $\underline{\underline{\varepsilon}}_\infty$ and the static dielectric tensor $\underline{\underline{\varepsilon}}_0$, the tensors of the oscillator strength for the axially polarized A_{2u} modes and the E_u modes polarized perpendicular to the c-axis have also been calculated.

The importance of the DF for the c-axis response and dielectric interlayer coupling, already evident for the A_{2u}^{Γ} modes shown in figure 1 and listed in table 1, can be checked for all the Λ_1 branches by inspection of the left-hand part of figure 2. The full lines represent the calculated Λ_1 branches for the AI model with DF included; the dotted curves, for comparison, give the results for the RIM and the dots show the neutron scattering results for insulating La_2CuO_4 [5, 18]. We find a considerable renormalization of the phonon frequencies by the DF, in particular for the high-frequency oxygen modes—i.e. the ferroelectric A_{2u}^{Γ} mode, the $A_{2u}^{\Gamma}(O \uparrow\downarrow)$ mode, where the apex oxygens O_z are displaced against the oxygen ions O_{xy} of the CuO_2 plane, and the axial oxygen breathing mode O_z^{Γ}. In the right-hand part of figure 2 the remaining calculated branches for the Λ direction Λ_2 (— — —) and Λ_3 (——) are shown and compared with experiment. In total, the calculated phonon dispersion of the AI model is in good agreement with the experiments and the electronic DF are essential for a quantitative description of the c-axis phonons and screening in La_2CuO_4 and very likely in the other HTSC as well.

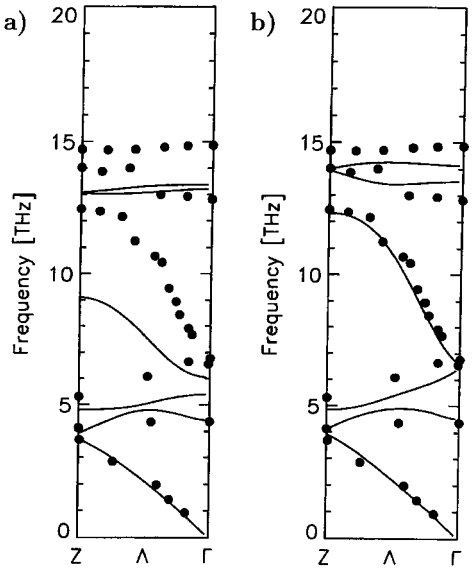

Figure 3. Calculated phonon dispersion for metallic La_2CuO_4 in the adiabatic approximation (static screening) of the Λ_1 branches. Part (*a*) shows the results for model AM1 and part (*b*) for model AM2, explained in the text. The dots give the experimental data [5, 17].

For the calculation of the Λ_1 phonons and the *c*-axis charge response of the doped metallic phase of La_2CuO_4, additionally to the DF we allow for electronic CF according to a model as proposed in [7] for the adiabatic approximation. In this investigation the polarizability given in equation (10) is based on a tight-binding representation of the first-principles band structure of [19] including La 5d, Cu 3d, 4s, 4p and O 2p states leading to a 31-band model (31 BM) that is typical for a LDA-like band structure. The effective ionic charges assumed in the RIM also have been calculated from this tight-binding band structure. Moreover, we have simplified this model, taking into account diagonal matrix elements of the polarizability only. With such a model (AM1), we obtain phonon dispersion curves which are in good agreement with those obtained from the complete polarizability matrix of the 31 BM. The result for the Λ_1 branches as calculated with model AM1 is shown in figure 3(*a*) (full curves) together with the experimental neutron data [5, 18]. From this calculation we deduce that screening along the *c*-axis is overemphasized by such a LDA-like model of the electronic charge response. In particular, the dispersion of the characteristic Λ_1 branch is far less steep than in the experiments; this originates from the fact that the LDA-based model AM1 overestimates the coupling along the *c*-axis and thus underestimates the anisotropy in La_2CuO_4.

A strictly two-dimensional electronic structure results in a much better modelling of the charge response along the *c*-axis. This can be achieved by neglecting in model AM1 the CF at the La and O_z ions in the ionic layers. So we get a strictly two-dimensional model (AM2) where only Cu 3d, 4s, 4p and O_{xy} 2p CF in the CuO_2 plane are allowed. With model AM2 we obtain a good agreement with the experiments—see figure 3(*b*)—in particular, the steep Λ_1 branch is in excellent agreement with the interpretation of the neutron data.

The A_{2u} splittings are closed in these calculations for the metallic phase in the adiabatic approximation (static response). Consistency is achieved with the interpretation of the neutron results, but not with the experimental evidence from infrared spectroscopy, which yields an insulator-like charge response, and as a consequence the dispersion of the Λ_1 branches should look like that in the left-hand part of figure 2.

From our calculation of the phonon dispersion in the adiabatic approximation so far, and also from that in [7], we find that screening in La_2CuO_4 and most probably in the other HTSC is best described by a two-dimensional electronic structure in the CuO_2 planes, leading to corresponding CF at the ions in the plane, and by anisotropic DF, where the dipole polarizability dominates along the (ionic) c-direction. What remains to be clarified is the apparent inconsistency between the neutron and infrared results.

3.2. Metallic versus insulator-like screening of the c-axis phonons

In [4] we have already studied qualitatively the anisotropy dependence of the c-axis phonon dispersion of La_2CuO_4 in terms of an extended eleven-band model (11 BM) for the CF. In this calculation we have generalized an 11 BM that represents the two-dimensional electronic structure of the CuO_2 plane in terms of Cu 3d and O_{xy} 2p orbitals by introducing suitable interlayer coupling in parametrized form. In this way it is possible to pass from the strictly two-dimensional nonadiabatic case of charge response to the less anisotropic three-dimensional nearly adiabatic situation. The interlayer coupling parameter, K, defines the width of the quasiparticle band along the c-direction and the position of the c-axis plasmon.

In the present calculation for the dynamical generalization of the electronic polarization $\Pi_{\kappa\kappa'}(\vec{q}, \omega)$ according to equation (10), additional to the CF according to the extended 11 BM we allow for anisotropic DF along the z-direction as calculated with the Sternheimer method. This makes the investigations quantitative and a direct comparison with the experiments becomes possible, as could be expected from the good results found in the adiabatic approximation (static response) of section 3.1. In relation to equation (10), it should be noted that electron correlations, for example taken into account within the Hubbard model, lead to an electronic quasiparticle band structure where the bandwidth and the Fermi velocity are reduced in comparison with those of a LDA-like electronic band structure [20]. On the other hand, such a reduced electronic quasiparticle band structure at the Fermi level in the (k_x, k_y) plane will increase the size of the nonadiabatic region around the c-axis, because the free-plasmon frequency is decreased. In this way the properties of the quasiparticles in the CuO plane influence the dynamical charge response perpendicular to the plane near the c-axis.

By increasing the interlayer coupling K (i.e. the strength of the coherent charge response) over a sequence of five models, M1–M5, we study the effect of the anisotropy and the position of the c-axis plasmon, separately, on the coupled phonon–plasmon modes of Λ_1 symmetry. We shall demonstrate that whether one gets metallic screening effects of the Λ_1 modes depends on the frequency of the c-axis plasmon in comparison to the phonon frequencies. Thus the dispersion may look like that of an insulator or that of a metal.

Model M1 in figure 4 corresponds to $K = 0$ and represents the limit of a strictly two-dimensional electronic quasiparticle band structure. The c-axis plasmon is soft ($\omega = 0$) because in this extremely anisotropic case there is no coherent contribution to the charge transport along the c-axis. In the other models, M2–M5 with decreasing anisotropy, we have chosen K in such a way that the free plasmon at Γ in the extended 11 BM is at about 1 THz (M2), 5 THz (M3), 10 THz (M4) and 18 THz (M5); see table 2. From this table we can also deduce that the screening effects related to the DF considerably reduce the frequency of the free plasmon in the extended 11 BM.

In figure 4 the effect of the anisotropy of the material expressed by the relative position of the c-axis plasmon with respect to the phonon frequencies as calculated with the extended 11 BM generalized with anisotropic DF is shown for different interlayer couplings with increasing magnitude (models M1–M5 from left to right in the figure). In the extreme anisotropic limit of a strictly two-dimensional band structure (M1) (an acoustic plasmon

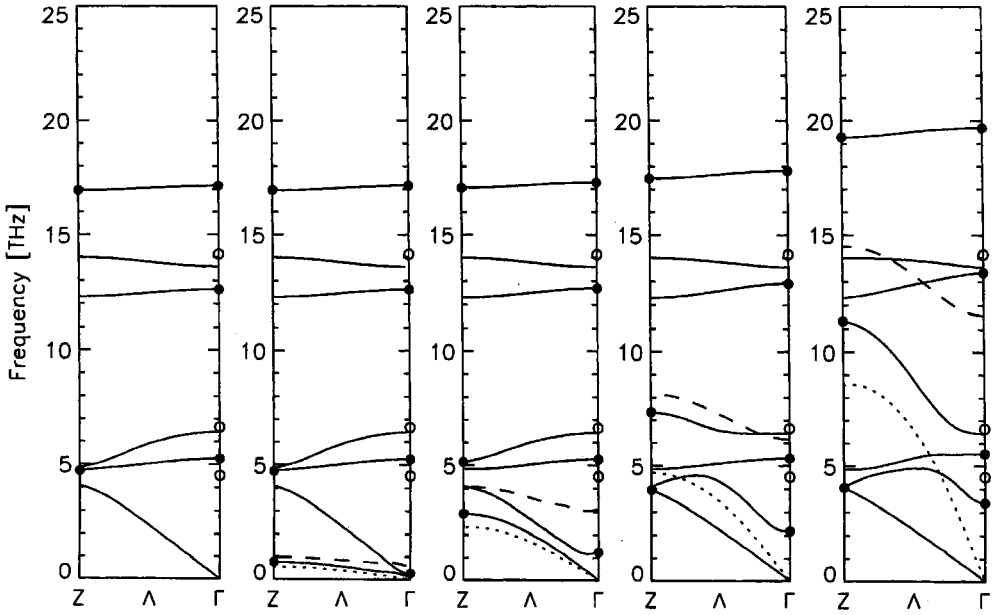

Figure 4. The effect of the anisotropy or the position of free-plasmon frequency on the phonon–plasmon scenario in La_2CuO_4 as calculated for different interlayer couplings with the extended eleven-band model including anisotropic DF. The models M1–M5, from left to right in the figure, are explained in the text. The open dots indicate the A_{2u}^{TO} modes at Γ.

Table 2. Free-*c*-axis-plasmon frequency in THz at the Γ and Z points of the Brillouin zone according to equation (11) for the extended 11 BM (CF) for different interlayer couplings (models M2–M5). The notation CDF represents the same models including, additionally, anisotropic DF.

	Γ point		Z point	
	CF	CDF	CF	CDF
M2	1.26	0.62	1.27	0.99
M3	5.05	3.11	5.26	4.09
M4	10.16	6.16	10.44	8.16
M5	18.75	11.58	18.30	14.49

when proceeding from the Λ direction to the $(q_x\ q_y)$ plane), the intraband contribution to the electronic polarizability Π vanishes for all wavevectors along the Λ direction in the dynamical (nonadiabatic) regime of screening. This means that the resulting phonon dispersion for the *metallic* phase cannot be distinguished from the dispersion of the *AI* in the left-hand part of figure 2. For this reason we call model M1 the *nonadiabatic insulator* model.

For very weak interlayer coupling, i.e. a large anisotropy (model M2), the plasmon-like Λ_1 branch is slightly below the free plasmon and consists of two parts of the two lowest Λ_1 branches. Note that because of the phonon–plasmon coupling, an additional branch appears in the nonadiabatic dispersion of the Λ_1 modes. So we have seven branches instead of the six branches in the adiabatic approximation and for model M1. For symmetry reasons the three LO A_{2u}^{Γ} modes and the two A_{1g}^{Z} modes, i.e. the axially symmetric apex-oxygen and La breathing modes O_z^Z and La_z^Z, are allowed to couple to the free plasmon at the Γ and the Z point, respectively. The latter are characterized as full dots in figure 4. The open dots indicate the A_{2u}^{TO} modes at Γ.

Except the lowest branch, the optical Λ_1 branches in M2 (phonon-like modes) are almost indistinguishable from those of the AI and the nonadiabatic insulator (M1), because in the case of a very low-lying plasmon as in model M2 (or M3) the slowly oscillating quasiparticles cannot screen the phonon-induced changes of the long-range Coulomb interactions between the ions. Thus, we will obtain optical activity also in the metallic state because the dynamical charge modulation is much slower than the motions of the ions. Moreover, we expect for highly anisotropic materials large contributions to the total self-consistent crystal potential $\delta V_\kappa(\vec{q}\sigma)$ in equation (15) from the phonon-like modes and this provides a favourable situation for pairing via nonlocal EPI of ionic origin [4]. The important role of a nonlocal long-ranged EPI in ionic polaron solids has also been emphasized in [22].

On the other hand, the high-frequency optical phonons are able to follow the slowly oscillating quasiparticles for a low-lying plasmon like in model M2 or M3. This leads to a further decrease of the already very low plasmon frequency in the form of a polaronic plasmon-like mode. We further expect damping effects of the quasiparticles via the strong nonlocal EPI of ionic origin and also via possible electronic correlation effects not considered in our model. Thus, damping or even overdamping of the very low-lying plasmon-like mode becomes very likely. In fact, experimentally the *c*-axis plasmon of metallic La_2CuO_4 seems to be strongly damped or even overdamped for $T > T_c$ [21, 23]. This indicates that the strong nonlocal EPI effects of ionic origin found in our calculations (see section 3.4), in addition to electronic correlation, may be an important aspect in understanding the confinement of the electrons in the CuO_2 planes.

Increasing the interlayer coupling (models M4 and M5 in figure 4), the plasmon-like branch is shifted through the spectrum to higher frequencies. The highest Λ_1 branch becomes plasmon-like and finally moves out of the spectrum towards the adiabatic limit for even larger coupling. Simultaneously, the dispersion of the phonon-like Λ_1 branches develops more and more adiabatic metallic character. In particular we see how the characteristic Λ_1 branch with the steep dispersion typical for the adiabatic metal is formed (model M5).

The scenario of phonon–plasmon mixing can be traced very well at the Z point because only the two modes La_z^Z and O_z^Z couple to the free plasmon. For a weak interlayer coupling (M2, M3), La_z^Z is mixed with the plasmon while with increasing interlayer coupling the character of the displacements of the plasmon-like mode changes. For model M4 the coupled mode is of mixed La_z^Z/O_z^Z type (at 7.36 THz) and for model M5 or even larger interlayer coupling the O_z^Z mode with the high frequency becomes plasmon-like, finally leaving the range of the phonon spectrum. At the Γ point the LO–TO splittings of the A_{2u}^Γ modes are closed from below with an increasing interlayer coupling.

Judging from the experimental evidence, i.e. the insulator-like infrared spectra independent of doping and a strongly damped or even overdamped plasmon, the very anisotropic models M1 or M2 are the most appropriate for an approximate description of the situation in La_2CuO_4 in the metallic phase within our theory. In particular, we deduce from our calculations the consistency of the measured (insulator-like) optical *c*-axis data with the calculated (insulator-like) phonon dispersion along the Λ direction for the metallic phase in these models. In the case of a stronger LDA-like interlayer coupling, i.e. a less anisotropic situation, the LO–TO splittings get closed—in contrast to the infrared data—because the optical phonons are sufficiently screened by the plasmon with a sufficiently high frequency. What still remains open is the question of why the current interpretation of the neutron result for the doped metallic phase looks like that calculated for an adiabatic metal.

3.3. Screening near to the c-axis

A possible explanation of the inconsistency of the current interpretation of the neutron scattering data and the optical infrared experiments follows from an investigation of the phonon

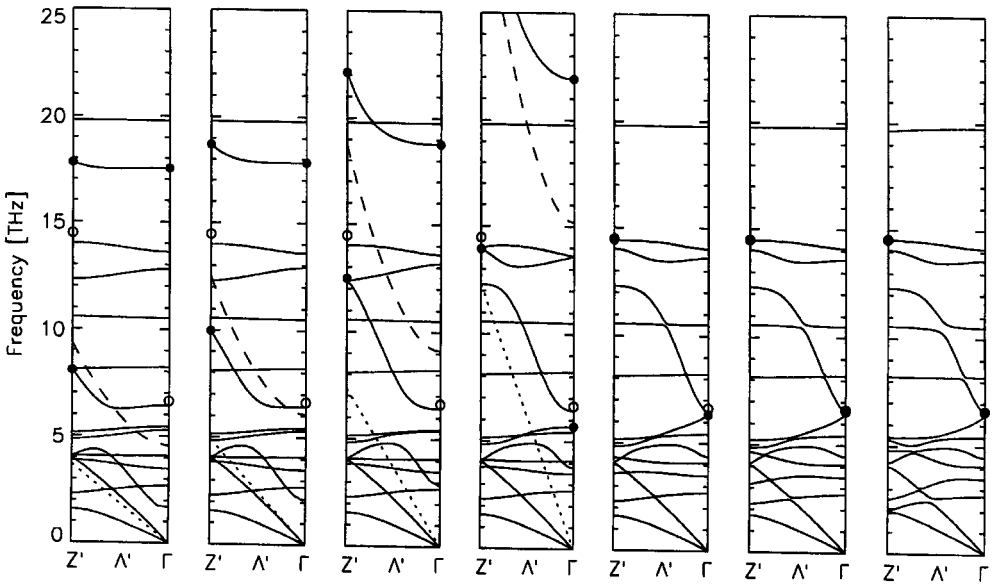

Figure 5. Nonadiabatic phonon dispersion as calculated with model M1 from Γ to $Z' = (\varepsilon\, 2\pi/a, 0, 2\pi/c)$ along the Λ' direction defined by $\vec{q} = \xi(\varepsilon\, 2\pi/a, 0, 2\pi/c)$ for different values of ε and $0 < \zeta \leqslant 1$ with $\xi_{\min} = 0.01$. From left to right we have in the panels of the figure: $\varepsilon = 0.003, 0.004, 0.006, 0.01, 0.025, 0.05, 0.1$. Only the Λ_1' branches (——) coupling to the CF are shown. – – –: free-plasmon branch; - - - -: borderline for damping. Dots at Z′: ●: $O_z^{Z'}$ (na); ○: $O_z^{Z'}$ (ad). Dots at Γ: ●: A_{2u}^{LO} (ferroelectric; na); ○: A_{2u}^{TO} (ferroelectric; ad). na: nonadiabatic; ad: adiabatic.

dispersion in a small region around the Λ direction. In principle—although not quantitative—such an explanation already has been provided in [4], where it has been demonstrated that in a small cone-like region around the Λ direction with $q_z \gg q_{x,y}$ dynamical coupling effects appear provided that the c-axis dispersion of the quasiparticle band structure is small enough. The charge response then is nonadiabatic and along the c-axis it is insulator-like as discussed in section 3.2. The following explanation for the observation of an adiabatic metallic phonon dispersion like in figure 3(b) was presented in [4].

In neutron scattering experiments a severe complication arises from the finite resolution in momentum transfer. The wavevector cannot resolved with sufficient precision along the Λ direction. In such a situation a relatively small nonadiabatic insulator-like part of the cone close to the c-axis would be outweighed in the measurement by a significantly larger part where the phonon dispersion is nearly adiabatic. Thus, in the neutron experiments, essentially the adiabatic, metallic dispersion with vanishing A_{2u} splittings and the typical Λ_1 branch with the steep dispersion would show up, just as is seen in figure 3(b).

In the following we reinvestigate the phonon dispersion around the c-axis with the quantitative model M1 including CF together with anisotropic DF not considered in [4], and determine the size of the region around Λ with an insulator-like, nonadiabatic charge response which is crucial to the argument above. This is done for a cone-like region as in [4] but also for a small tube around Λ. The latter calculation is better adapted to the experimental situation, because the wavevector resolution perpendicular to the Λ direction remains constant all the way along the c-axis.

A representative direction for the cone is the direction $\Lambda' \sim (\varepsilon\, 2\pi/a, 0, 2\pi.c)$ where ε determines the angle $\alpha(\varepsilon)$ between the Λ direction and Λ' and gives a measure for the size

of the cone. Only fourteen phonon branches of Λ_1' symmetry couple to the CF. In figure 5 the nonadiabatic phonon dispersion of these Λ_1' branches as calculated with the model M1 are displayed for different values of ε increasing from left to right in the panels of the figure. Increasing ε or $\alpha(\varepsilon)$ rapidly moves the free-plasmon mode (broken curve) out of the phonon spectrum as a consequence of the quasiparticle dispersion in the (k_x, k_y) plane. For ε between 0.006 and 0.01 we find a region of crossover from nonadiabatic insulator-like to adiabatic metallic charge response. The characteristic branch with the steep dispersion appearing in the adiabatic calculation is already seen for $\varepsilon = 0.006$. The transition from the nonadiabatic to the adiabatic regime can be traced very well by following the $O_z^{Z'}$ mode in figure 5. For $\varepsilon \lesssim 0.004$ the lower of the two coupled $O_z^{Z'}$ modes (full dots) is plasmon-like. On increasing ε successively, this mode approaches its adiabatic value (open dot), thereby changing its character to phonon-like. Simultaneously the higher of the two modes, which is for small ε-values phonon- and insulator-like, is shifted out of the spectrum together with the free plasmon and changes its character to plasmon-like. A similar behaviour can be assigned to the longitudinal A_{2u} modes at Γ. For small values of ε we find a typical insulator-like charge response characterized by a large splitting of the 'ferroelectric mode' (full and open dots at Γ). On increasing ε, the LO–TO splitting is closed from below. The phonon-like A_{2u}^{LO} (ferroelectric) mode can be identified only for $\varepsilon \approx 0.01$ and larger values, because for smaller ε the lower A_{2u}^{LO} modes are of mixed character. So we have shown in figure 5 for $\varepsilon < 0.01$ the higher A_{2u}^{LO} (ferroelectric) mode only, which becomes plasmon-like for larger ε and finally leaves the spectrum together with the free plasmon.

Note that the effective interaction between the electrons in the case where phonon–plasmon coupling is present is attractive in the frequency range between the A_{2u}^{TO} (ferroelectric) mode and the higher A_{2u}^{LO} (ferroelectric) mode. Thus, the large splitting of this mode is favourable for pairing and the role played in this 'game' by the imperfectly screened long-ranged Coulomb interaction in the nonadiabatic regime along the c axis again becomes evident. On the other hand, such a pairing channel is not possible in conventional high-density metals and superconductors.

In figure 6 we have displayed the nonadiabatic phonon dispersion as calculated with model M1 along the Λ'' direction parallel to the c-axis. The discussion of the transition from the nonadiabatic regime for small ε to the adiabatic regime for larger ε is similar to that in relation to the cone. In particular, we see a strong increase of the free-plasmon frequency when going away from the c-axis, and as a consequence the charge response rapidly becomes more and more adiabatic (metallic). Again we find a region of crossover from nonadiabatic insulator-like behaviour to adiabatic metallic behaviour for ε between 0.006 and 0.01 and the characteristic branch with the steep dispersion appears at $\varepsilon \approx 0.006$.

From both of our calculations in figures 5 and 6 we deduce a narrow region in reciprocal space around the c-axis of insulator-like charge response. Typically at $\varepsilon \approx 0.006$ metallic behaviour starts to dominate. According to [24] the experimental wavevector resolution perpendicular to the Λ direction is on average $\varepsilon = 0.03$. Thus, the off-axis phonons from the region with a metallic charge response dominate the neutron scattering cross section in the experiments and the c-axis dispersion looks metallic despite an insulating response behaviour for the phonons propagating strictly along the c-axis and within the small nonadiabatic part of the cone or tube.

Another interesting feature of the nonadiabatic results and the phonon–plasmon scenario is the strong increase with ε of the plasmon-like $O_z^{Z'}$ mode towards its adiabatic value in figures 5 and 6. Put differently, there is a rapid shooting down of $O_z^{Z'}$ when approaching the Z point which arises from the nonadiabatic dynamic charge–lattice coupling. Experimentally a strong softening of about 6 THz of the nearby symmetrical apex-oxygen breathing mode at the

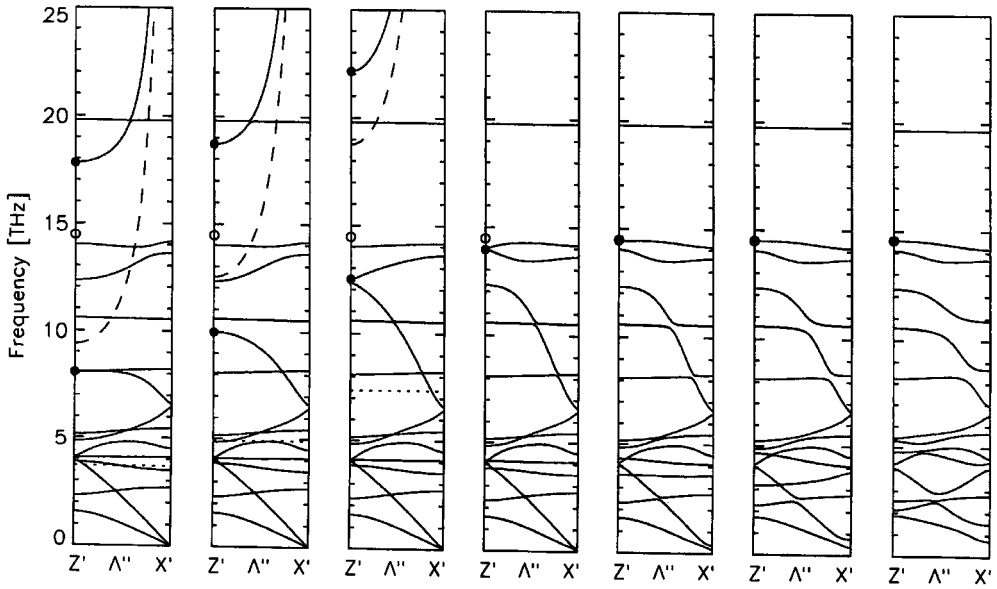

Figure 6. Nonadiabatic phonon dispersion as calculated with model M1 from $X' = (\varepsilon\, 2\pi/a, 0, 0)$ to Z' along the Λ'' direction defined by $\vec{q} = (\varepsilon\, 2\pi/a, 0, \zeta 2\pi/c)$ parallel to the c-axis for different values of ε and $0 < \zeta \leqslant 1$ with $\xi_{\min} = 0.01$. From left to right we have in the panels of the figure: $\varepsilon = 0.003, 0.004, 0.006, 0.01, 0.025, 0.05, 0.1$. Only the Λ'' branches (——) coupling to the CF are shown. – – –: free-plasmon branch; - - - -: borderline for damping. Dots at Z': ●: $O_z^{Z'}$ (na); ○: $O_z^{Z'}$ (ad).

Z point, O_z^Z, is observed when going from insulating La_2CuO_4 ($\approx$17 THz) to optimally doped metallic $La_{1.85}Sr_{0.15}CuO_4$ ($\approx$11 THz) [25]. However, in the optimally doped probe a large line broadening of about 4 THz has also been found, that makes it difficult to measure the exact position of O_z^Z in the metallic phase. From the theoretical side, such a strong renormalization for O_z^Z during the insulator–metal transition was predicted in [13], representing the insulating phase by the RIM and taking only CF as screening processes in the metallic phase into account. From the present more quantitative calculations in the adiabatic approximation shown in figures 2 and 3, we find that the softening arising from the Coulomb coupling of the CF in different layers alternating in sign is reduced to about 3 THz, but is still large. In the superconducting state the Coulomb coupling between the CF of opposite signs in different layers as generated by the $O_z^{Z'}$-like modes supports pairing in the CuO planes.

In the insulating phase we get for O_z^Z 16.95 THz (in good agreement with the experiment) as compared to 19.36 THz in the RIM because of a strong renormalization by anisotropic dipole screening. In the metallic phase we have for O_z^Z 13.95 THz in model AM1, which is higher than the experimental guess for this mode. The experimentally observed large width of O_z^Z and the uncertainty of its position in the metallic phase can now be understood in the phonon–plasmon scenario and supposed also to be due to the limited wavevector resolution perpendicular to the c-axis in the experiments. In this case the experiment picks up, for the neutron cross section, the contributions from the plasmon-like $O_z^{Z'}$ modes varying strongly in frequency near to the Z point. So we obtain in our calculations for $O_z^{Z'}$ an increase as follows: for $\varepsilon = 0.003$ we have about 8 THz, for $\varepsilon = 0.004$ about 10 THz and for $\varepsilon = 0.006$ about 12.5 THz; see figures 5 and 6. Thus, the existence of the phonon–plasmon coupling is also supported by the experimental behaviour of the O_z^Z mode.

3.4. Nonlocal electron–phonon interaction of ionic origin

In this last section we investigate the effect of the anisotropy and of phonon–plasmon coupling on the magnitude of the self-consistent changes of the nonlocally induced crystal potential $\delta V_\kappa(\vec{q}\sigma)$ according to equation (15). $\delta V_\kappa(\vec{q}\sigma)$ represents the EPI in a particular mode and its magnitude gives a measure of the contribution of that mode to the pairing mechanism. For our investigations we apply the models M1–M5 and compare with the adiabatic calculation (AD). As typical modes from the nonadiabatic region of charge response we focus on the axial oxygen and the axial lanthanum breathing modes at the Z point, O_z^Z and La_z^Z. Here we have the situation that the displacements of ions (O_z, La) in the ionic layers generate changes of the potential felt by the electrons in the CuO_2 plane which themselves are responsible for the superconductivity. Such nonlocal coupling effects are due to the strong component of the ionic binding along the *c*-axis in the HTSC, i.e. these Coulomb coupling effects are very special to this class of materials, and would not be possible in a conventional metal or superconductor because the changes of the potential generated by the displaced ions would be locally screened by a high-density electron gas.

In table 3 the results for $|\delta V_\kappa|$ for the La_z^Z and O_z^Z modes are listed for the models M1–M5 and the AD for comparison. In the case of an extreme or a very large anisotropy, the free-plasmon frequency including DF is below 5 THz (models M1–M3). The low-lying plasmon-like mode appearing in M2 or M3 can be assumed to be strongly damped or overdamped in La_2CuO_4 on the basis of the experiments [21,23], as already mentioned. Thus, this, in addition to the phonons (in principle, very effective) plasmon-like coupling channel for pairing with large values for $|\delta V_\kappa|$ (see table 3), is not realistic for La_2CuO_4. However, because of the insulator-like charge response, we obtain a large coupling via the phonon-like channel in the highly anisotropic situation. For example, we get from table 3 for the O_z^Z mode in model M2 $|\delta V(\text{Cu 3d})| \approx 348$ meV as compared to $|\delta V(\text{Cu 3d}) \approx 14$ meV in the adiabatic calculation with static metallic screening. Therefore a favourable situation for pairing is provided by the phonon-like modes in the case of a large anisotropy.

For an interlayer coupling as obtained with models M4 and M5, i.e. for a more moderate anisotropy, we find from table 3 large contributions for $|\delta V_\kappa|$ from the plasmon-like and the phonon-like modes. In particular, for the less anisotropic regime described by M5 and for larger interlayer couplings as in the LDA-like calculations [17], the plasmon-like coupling channel dominates. In total, these studies support the more qualitative calculations given in [4] where DF are neglected.

4. Summary

Our calculations have shown that La_2CuO_4 is best described by a two-dimensional electronic structure of the CuO_2 plane and with CF at the Cu and O_{xy} ions as the most important screening process in the plane. Screening along the ionic *c*-direction between the layers is essentially of dipole type and can quantitatively be represented by anisotropic DF. Modelling the charge response along these lines yields a calculated phonon dispersion which is in good agreement for both the insulating and metallic phase. This means that even if the single-particle hopping between the CuO_2 planes is negligible (like in the Luttinger-liquid picture), the three dimensionality due to direct Coulomb interaction and dielectric coupling between the layers is important.

We have shown that the charge transport strictly along the *c*-axis is (nonadiabatic) insulator-like because of the large anisotropy of the material and so we can deduce the consistency of the measured (insulator-like) optical infrared data with the calculated phonon dispersion along the Λ direction for the metallic phase.

Table 3. Magnitudes of the phonon-induced changes of the self-consistent crystal potential δV_κ according to equation (15) for the O_z^Z and La_z^Z mode in units of meV at the Cu and O_{xy} ions in the CuO_2 plane. The models M1–M5 are explained in the text. The coupled-mode frequencies and that of the free plasmon at the Z point, ν_{pl}, are in THz. In the case where Im $\delta V_\kappa \neq 0$, which is possible for phonon modes in the damping region (models M4, M5), the magnitude of the imaginary part is given in a second row. pl: plasmon-like; ph: phonon-like; AD: adiabatic.

	ν_{pl}	ν	Cu	O_{xy}	
M1	—	4.72	140.06	198.35	La_z^Z
		16.95	347.34	343.95	O_z^Z
M2	0.99	0.78	1070.23	470.96	La_z^Z (pl)
		4.73	144.01	200.76	La_z^Z (ph)
		16.98	348.27	344.65	O_z^Z
M3	4.09	2.91	292.85	64.54	La_z^Z (pl)
		5.14	239.40	258.66	La_z^Z (ph)
		17.07	364.17	356.60	O_z^Z
M4	8.16	3.95	43.27	82.42	La_z^Z
			30.96	19.13	
		7.36	644.69	485.92	O_z^Z/La_z^Z
		17.48	422.85	400.71	O_z^Z
M5	14.49	4.06	18.56	102.30	La_z^Z
			21.10	12.49	
		11.33	445.14	262.86	O_z^Z (ph)
		19.27	677.96	592.85	O_z^Z (pl)
AD	∞	4.09	13.65	107.04	La_z^Z
		14.47	13.72	78.76	O_z^Z

An explanation of the apparent inconsistency between the current interpretation of the neutron scattering results for the Λ_1 branches in doped metallic samples that look like those expected for a less anisotropic metal and the infrared data being typical for an ionic insulator has been presented within a quantitative model including CF and DF. This has been achieved by calculating the size of the region around the c-axis where an insulator-like nonadiabatic charge response occurs. This region is shown to be very small. Outside it the charge response is essentially adiabatic metallic and screening becomes more effective. The finite resolution of the wavevector in the experiment then leads to the region with a metallic response dominating the neutron scattering cross section, and the c-axis phonon dispersion looks metallic despite the insulating behaviour of the phonons propagating strictly along the c-axis or in the insulator-like part of reciprocal space nearby. Moreover, we have presented arguments to help in understanding the large softening and the massive line broadening of the O_z^Z mode experimentally observed in relation to the phonon–plasmon coupling.

Finally, we have discussed the effect of anisotropy and phonon–plasmon mixing on the nonlocal electron–phonon coupling of ionic origin. We find a large increase of coupling via the phonon-like channel in the highly anisotropic situation while for the less anisotropic LDA-like case the plasmon-like channel dominates.

Long-range Coulomb interactions and their screening with doping in terms of CF that are controlled by the interplay of strong local interactions and effects of the kinetic energy are a crucial aspect in understanding the physics in the HTSC. This picture has become evident

during the investigation of other relevant phonon modes with a strong nonlocal EPI in the adiabatic regime in addition to that from the nonadiabatic region near to the *c*-axis studied in this paper. The phonon modes in question are the high-frequency copper–in-plane-oxygen bond-stretching vibrations investigated in [11, 26–28]. The phase space for strong nonlocal coupling by these modes has been shown to be large [26] and the latter are now thought to cause a kink in the electronic dispersion observed by means of photoemission [29], which also suggests strong EPI. Moreover, the induced electronic charge redistributions excited by these modes have the form of one-dimensional dynamical charged stripes of CF with alternating sign along the (1, 0, 0) and (1, 1, 0) directions, expressing the importance of interactions between localized charge and lattice fluctuations. Note that also the effective spin-exchange interaction between neighbouring Cu orbitals is modulated by the oxygen displacement [30] and, in this way, spin degrees of freedom may also enter the scenario via the high-frequency copper–in-plane-oxygen bond-stretching modes. Moreover, the antiferromagnetic structure favours the CF in a spin-correlated system (with coupled spin and charge variables), because if the spins in neighbouring Cu orbitals were to be parallel, they would not both be able to transfer to the oxygen or between themselves; on the other hand, if they are antiparallel, they can. So we will have both CF and spin fluctuations induced by the lattice vibration. In the superconducting state, the strong charge modulation of alternating sign in the (1, 0, 0) directions energetically favours pairing along the CuO bonds (in the case where the doped carriers predominantly go to the oxygen site) while, as mentioned above, the $O_z^{Z'}$-like modes simultaneously favour pairing to the plane.

From the experiments and from our investigations, it can be concluded that the unusual nonlocal EPI of ionic origin strongly influences the electron dynamics in the HTSC. This underlines the importance of that type of EPI in the pairing mechanism of the HTSC.

Acknowledgment

We greatly appreciate the financial support by the Deutsche Forschungsgemeinschaft.

References

[1] Pickett W 1989 *Rev. Mod. Phys.* **61** 433
[2] Anderson P W 1997 *The Theory of Superconductivity in the High-T_c Cuprates* (Princeton, NJ: Princeton University Press)
[3] Radtke R J, Kostur V N and Levin K 1996 *Phys. Rev.* B **53** R522
[4] Falter C, Klenner M and Hoffmann G A 1998 *Phys. Rev.* B **57** 14 444
[5] Pintschovius L and Reichardt W 1994 *Physical Properties of High Temperature Superconductors IV* ed D M Ginsberg (Singapore: World Scientific)
[6] Alexandrov A S 1992 *Phys. Rev.* B **46** 2838
[7] Falter C and Schnetgöke F 2002 *Phys. Rev.* B **65** 054510
[8] Uchida S, Tamasaku K and Tajima S 1996 *Phys. Rev.* B **53** 14 558
[9] Henn R, Kircher J and Cardona M 1996 *Physica* C **269** 99
[10] Henn R, Wittlin A, Cardona M and Uchida S 1997 *Phys. Rev.* B **56** 6295
[11] Falter C, Klenner M and Ludwig W 1993 *Phys. Rev.* B **47** 5390
[12] Falter C, Klenner M, Hoffmann G A and Schnetgöke F 1999 *Phys. Rev.* B **60** 12 051
[13] Falter C, Klenner M and Hoffmann G A 1995 *Phys. Rev.* B **52** 3702
[14] Mahan G D 1980 *Phys. Rev.* A **22** 1780
[15] Mahan G D and Subbaswamy 1990 *Local Density Theory of Polarizability* (New York: Plenum)
[16] Krakauer H, Pickett W E and Cohen R E 1988 *J. Supercond.* **1** 111
[17] Falter C, Klenner M and Hoffmann G A 1998 *Phys. Status Solidi* b **209** 235
[18] Chaplot S L, Reichardt W, Pintschovius L and Pyka N 1995 *Phys. Rev.* B **52** 7230
[19] DeWeert M J, Papaconstantopoulos D A and Pickett W E 1989 *Phys. Rev.* B **39** 4235

[20] Dopf G, Wagner J, Dieterich P, Muramatsu A and Hanke W 1992 *Phys. Rev. Lett.* **68** 2082
[21] Tamasaku K, Nakamura Y and Uchida S 1992 *Phys. Rev. Lett.* **69** 1455
[22] Alexandrov A S 2000 *Phys. Rev.* B **61** 12 315
[23] Kim J H, Somal H S, Czyzyk M T, van der Marel D, Wittlin A, Gerrits A M, Duijn V H M, Hien N T and Menovsky A A 1995 *Physica* C **247** 297
[24] Pintschovius L 1999 private communication
[25] Pintschovius L and Reichardt W 1998 Neutron scattering in layered copper-oxide superconductor *Physics and Chemistry of Materials with Low Dimensional Structures* vol 20, ed A Furrer (Dordrecht: Kluwer)
[26] Falter C and Hoffmann G A 2001 *Phys. Rev.* B **64** 54 516
[27] Falter C, Klenner M, Hoffmann G A and Chen Q 1997 *Phys. Rev.* B **55** 3308
[28] Falter C and Hoffmann G A 2000 *Phys. Rev.* B **61** 14 537
[29] Lanzara A *et al* 2001 *Nature* **412** 510
[30] Lorenzana J and Sawatzky G A 1995 *Phys. Rev. Lett.* **74** 1867